European Journal of Pharmaceutics and Biopharmaceutics 94 (2015) 180–193

Contents lists available at ScienceDirect

European Journal of Pharmaceutics and Biopharmaceutics

journal homepage: www.elsevier.com/locate/ejpb

Research Paper

Intranasal delivery of dopamine to the striatum using glycol chitosan/sulfobutylether-β-cyclodextrin based nanoparticles

Sante Di Gioia [a], Adriana Trapani [b,*], Delia Mandracchia [b], Elvira De Giglio [c], Stefania Cometa [c], Vincenzo Mangini [c], Fabio Arnesano [c], Giuliana Belgiovine [a], Stefano Castellani [a], Lorenzo Pace [d], Michele Angelo Lavecchia [e], Giuseppe Trapani [b], Massimo Conese [a], Giovanni Puglisi [f], Tommaso Cassano [d]

[a] Department of Medical and Surgical Sciences, University of Foggia, Viale L. Pinto 1, 71122 Foggia, Italy
[b] Department of Pharmacy-Drug Sciences, University of Bari "Aldo Moro", via Orabona, 4, 70125 Bari, Italy
[c] Department of Chemistry, University of Bari "Aldo Moro", via Orabona, 4, 70125 Bari, Italy
[d] Department of Clinical and Experimental Medicine, University of Foggia, Viale L. Pinto 1, 71122 Foggia, Italy
[e] Department of Physiology and Pharmacology "V. Erspamer", Sapienza University of Roma, Piazzale A. Moro 5, 00185 Roma, Italy
[f] Laboratory of Drug Delivery Technology, Department of Drug Sciences, University of Catania, Viale A. Doria 6, 95125 Catania, Italy

ARTICLE INFO

Article history:
Received 18 December 2014
Revised 23 April 2015
Accepted in revised form 9 May 2015
Available online 30 May 2015

Chemical compounds studied in the article:
Dopamine hydrochloride (PubMed CID: 65340)
L-Dopa (PubMed CID: 6047)
Chitosan (PubMed CID: 71853)
Pentasodium tripolyphosphate (PubMed CID: 24455)
Fluorescein isothiocyanate (PubMed CID: 18730)
Noradrenaline (PubMed CID: 439260)
Dihydroxyphenylacetic acid (PubMed CID: 547)
β-Cyclodextrin (PubMed CID: 444041)

Keywords:
Brain delivery
Dopamine
Chitosan/glycol chitosan
Nanoparticles
XPS (X-ray photoelectron spectroscopy)
Nasal administration

ABSTRACT

The aim of this study was to evaluate chitosan (CS)-, glycol chitosan (GCS)- and corresponding thiomer-based nanoparticles (NPs) for delivering dopamine (DA) to the brain by nasal route. Thus, the polyanions tripolyphosphate and sulfobutylether-β-cyclodextrin (SBE-β-CD), respectively, were used as polycation crosslinking agents and SBE-β-CD also in order to enhance the DA stability. The most interesting formulation, containing GCS and SBE-β-CD, was denoted as DA GCS/DA-CD NPs. NMR spectroscopy demonstrated an inclusion complex formation between SBE-β-CD and DA. X-ray photoelectron spectroscopy analysis revealed the presence of DA on the external surface of NPs. DA GCS/DA-CD NPs showed cytotoxic effect toward Olfactory Ensheathing Cells only at higher dosage. Acute administration of DA GCS/DA-CD NPs into the right nostril of rats did not modify the levels of the neurotransmitter in both right and left striatum. Conversely, repeated intranasal administration of DA GCS/DA-CD NPs into the right nostril significantly increased DA in the ipsilateral striatum. Fluorescent microscopy of olfactory bulb after acute administration of DA fluorescent-labeled GCS/DA-CD NPs into the right nostril showed the presence of NPs only in the right olfactory bulb and no morphological tissue damage occurred. Thus, these GCS based NPs could be potentially used as carriers for nose-to-brain DA delivery for the Parkinson's disease treatment.

1. Introduction

Parkinson's disease (PD) is characterized by a progressive degeneration of dopaminergic neurons in the nigrostriatal track and a decrease of striatal Dopamine (DA) availability [1]. PD affects 1–2% of individuals over 60 years and its incidence is supposed to increase especially for an enhancement of life expectancy and greater aging population. Currently, L-Dopa is the drug of choice for many PD patients and, following oral administration, it is able to alleviate the symptoms for many years. However, after long-term treatment, many PD patients develop motor response fluctuations and involuntary movements called "L-Dopa-induced dyskinesia", which may be more disabling than parkinsonism

* Corresponding author. Tel.: +39 0805442114; fax: +39 0805442724.
E-mail address: adriana.trapani@uniba.it (A. Trapani).

http://dx.doi.org/10.1016/j.ejpb.2015.05.019
0939-6411/

[2,3]. Consequently, there is a need to develop alternative therapeutic strategies focused on both symptomatic and disease-modifying or neuroprotective treatments [4].

The treatment of PD by exogenous administration of DA is hampered by its inability to overcome the blood brain barrier (BBB) [5]. As well documented, the physiological role of the BBB is to maintain brain homeostasis allowing the transport of nutrients and the exclusion of toxic substances from the brain. The BBB consists of a complex of brain capillary endothelial cells fused by tight junctions together with pericytes, astroglial and perivascular macrophages. Consequently, the BBB shows low paracellular permeability and only small lipophilic molecules are able to overcome it by transcellular passive diffusion. In addition to its low paracellular permeability, the BBB also expresses a high number of efflux transporters including P-glycoprotein (P-gp/MDR1), breast cancer resistance protein and the multi-drug resistance-associated protein family, which limit the distribution of drugs in the brain [6,7].

The DA inability to overcome the BBB is mainly attributed to its unfavorable physicochemical features as high hydrogen bonding potential and complete ionization at physiological pH and, moreover, it is extensively metabolized by liver when orally administered [5,8]. Instead of the oral and intravenous route, the intranasal drug administration is receiving great consideration as a promising pharmacokinetic approach for the PD treatment. To this regard, de Souza Silva and colleagues, for the first time, showed by *in vivo* microdialysis that intranasal administration of dopaminergic drugs such as the psychostimulants cocaine and amphetamine or the antiparkinsonian drug L-Dopa can increase extracellular DA levels in the striatum [9,10]. These interesting results have encouraged further to pursuit of this approach. In fact, more recently many authors have investigated the effects of DA or L-Dopa intranasally applied [11–17]. Moreover, the intranasal administration has been used by different authors to test the prion-like spreading of pathological α-synuclein in the brain [18–21]. In particular, it has been reported that nasal administration of α-syn amyloidogenic species produce dopaminergic but also non-dopaminergic parkinsonian neurochemical alterations as well as behavioral deficits indicated by rigidity and reduced locomotor activity [18–20]. In this respect, it has been demonstrated that there is a final common pathway linking olfactory neuroepithelial receptor cells with axonal projections of the olfactory bulb and these networks are connected to centrifugal neuronal afferents from the substantia nigra dopamine nuclei [22]. Therefore, intranasal route is a non-invasive method of drug delivery, which may bypass the BBB enabling a direct access to the Central Nervous System (CNS) for therapeutic substances [6]. Autoradiographic studies with [^{3}H] DA have clearly shown that the neurotransmitter is transferred into the olfactory bulb after nasal administration and then reaches the CNS [23]. Several studies showed that the transport of DA at central level is carrier-mediated. Thus, DA may be transported into the brain exploiting the "Large neutral Amino acid" Transporter (LAT) carrier which is able to transport not only L-Dopa but also other aminoacid-related compounds as DA [24]. In addition, Chemuturi and colleagues described enhanced CNS uptake of DA following intranasal administration due to the presence of DA Transporter (DAT) and Organic Cation Transporter-2 (OCT-2) in the nasal mucosa [5,25]. Moreover, DA is metabolized in limited extent by the nasal mucosa to its main metabolite dihydroxyphenylacetic acid (DOPAC) [26].

In general, the CNS bioavailability following nasal administration is affected by some physiological factors including rapid mucociliary clearance from the nasal cavity and susceptibility to degradation due to the presence of metabolizing enzymes in the nasal epithelium such as Cytochrome P450 and NADPH-cytochrome P450 reductase, while the occurrence of the monoamino oxidase in the nasal mucosa is still questioned [26,27]. It should be also taken into account that: (*i*) there is the need to avoid irritation of the nasal mucosa considering that the normal pH in the nasal cavity is between 5.5 and 6.0 [28,29]; (*ii*) to increase the bioavailability up to 20–68%, it is necessary to co-administer absorption enhancers including chitosan, polyethylene glycol and cyclodextrins (CDs) [29–31]; (*iii*) nanovectors improve nasal drug delivery because they can protect the encapsulated drug from chemical degradation and can modulate or reverse the effect of the efflux pumps [32]; (*iv*) nanovectors constituted by mucoadhesive polymers can improve the bioavailability because allow a greater contact with the nasal mucosa and, hence, prolonged residence times at the absorption site [33].

Among the nanovectors potentially useful for nasal administration, polymeric nanoparticles (NPs) based on the biodegradable and mucoadhesive polymer chitosan (CS), have already been investigated for the DA delivery to CNS by parenteral route [8,34]. Besides intrinsic properties of the polycation, including low toxicity, excellent biocompatibility and mucoadhesive properties, CS also allows increased permeability of the nasal epithelia to drugs due to tight junction opening between apical cells [32]. However, a major drawback of CS is constituted by its poor water solubility at pH greater than 6.5 and many efforts have been carried out to overcome this problem [29]. Among the CS derivatives endowed with improved solubility, most interest is focused to glycol chitosan (GCS), which is water soluble at neutral/acidic pH values due to a hydrophilic ethylene glycol group introduced. On the other hand, in recent years, the mucoadhesive properties of CS have been strongly improved by immobilization of sulphydryl bearing ligands on the polycation, providing so CS derivatives named "thiomers" [35]. In this context, we have recently reported that CS- and GCS-based thiomers such as chitosan-*N*-acetyl-cysteine (CS-NAC), chitosan-glutathione (CS-GSH) and the corresponding conjugates with GCS (*i.e.*, GCS-NAC and GCS-GSH) are characterized by optimal-excellent mucoadhesive properties and, moreover, GCS-NAC 400 kDa and GCS 400 kDa, are able to inhibit the activity of the efflux pump P-gp/MDR1 [36].

The aim of the present work was to evaluate CS derivative-based NPs as nanocarriers for direct nose-to-brain DA delivery along the olfactory pathway following nasal administration. For this purpose, a number of NPs were prepared and characterized *in vitro* from the physicochemical point of view and neurotransmitter loading and release. The most interesting formulation has been further characterized by different analytical methods in order to evaluate both the location of the DA molecule in the nanocarrier and the interactions between the neurotransmitter and formulation components. Then, to assess whether the acute and repeated (every other day for 14 days) intranasal administration of DA loaded CS derivative-based NPs influence brain dopaminergic content, we measured the level of DA in the striatum of rats. We have focused on this brain region since it is widely acknowledged that the striatum is the main recipient of afferents from the basal ganglia and, moreover, as above mentioned, the most important neuropathological alteration in PD is the loss of dopaminergic neurons of the Substantia Nigra, which causes a severe depletion in striatal DA [1]. We have also investigated the impact of treatment on DA-turnover measuring the striatal DOPAC level. In this regard, we and other researchers have previously demonstrated that L-Dopa treatment enhanced DA metabolism, indicating that the conversion of L-Dopa into DA is accompanied by a higher DA metabolism, which may explain the gradual loss of L-Dopa efficacy over the time [37–39].

Moreover, noradrenergic pathways have a significant role in regulating basal ganglia function, and more interestingly, it has been reported that noradrenaline (NA) is synthesized from exogenous L-Dopa administered in PD therapy [40]. Therefore, we

assessed whether intranasal administration of DA-loaded CS derivative-based NPs could cause an increase of striatal NA as well as DA levels.

2. Materials and methods

2.1. Materials and animals

Chitosan hydrochloride (UP CL 113, MW 110 kDa, deacetylation degree 86%) was purchased from Pronova Biopolymer (Norway). Glycol Chitosan (MW 400 kDa according to supplier instructions), DA hydrochloride, fluorescein isothiocyanate (FITC) and pentasodium tripolyphosphate (TPP) were purchased from Sigma–Aldrich, Italy. Sulfobutylether-β-cyclodextrin sodium salt (SBE-β-CD, MW 2163 Da, average substitution degree 6.40) was purchased from CyDex, Inc. (USA). All other chemicals were reagent grade. Ultrapure water was used throughout the study. Synthesis and characterization of the conjugates CS-NAC, CS-GSH and GCS-NAC were carried out as previously described [36].

Male Wistar rats (225–250 g; Harlan, San Pietro al Natisone, Udine, Italy) were housed on 12-h dark-light cycle, at 22 ± 1 °C with food and water available ad libitum and habituated to housing conditions for 1 week before the experiments. Animal care and all experiments were conducted in accordance with the guidelines of the European Communities Council Directive of 24 November 1986 (86/609/EEC) and the Italian Department of Health (D.L. 116/92), and approved by the Institutional Animal Care and Use Committees of the University of Foggia, Italy. All efforts were made to minimize animal suffering and to reduce the number of animals used in the study.

2.2. Nanoparticle preparation

All the manipulations involving DA were carried out under light protection by using vessels covered with aluminum foils.

(a) General procedure for DA encapsulated in CS derivative-based NPs using TPP as crosslinking agent:

A 0.2% w/v solution of CS derivative was prepared in aqueous AcOH (0.1%. v/v). Then, DA was dissolved in the polysaccharide solution to achieve the final concentration of 0.5% w/v. To 0.75 ml of the resulting solution, an aqueous solution of TPP (0.07%, w/v) was added to induce NP formation. In particular, the volumes of TPP solution required to induce the gelation process were as follows: 0.8 ml for GCS, CS-NAC and GCS-NAC, 0.5 ml for CS-GSH.

(b) General procedure for DA adsorbed on CS derivative-based NPs using TPP as crosslinking agent:

These nanocarriers were prepared according to a previously reported procedure [8]. Briefly, to 0.75 ml of CS-, or GCS-, or corresponding thiomers-solution (0.2% w/v) in aqueous AcOH (0.1% v/v), an aqueous solution of TPP (0.07%, w/v) was added under magnetic stirring to induce the ionic gelation of the polycation. In detail, the volumes of TPP solution required to induce the gelation process were as follows: 0.8 ml for GCS, CS-NAC and GCS-NAC; 0.5 ml for CS-GSH. The resulting plain NPs, referred to as "unloaded NPs", were let at 25 °C to incubate in a water shacked bath (100 rpm/min) in the dark for 3 h with 2 ml of 0.5% w/v DA aqueous solution.

(c) General procedure for DA encapsulated in CS derivative-based NPs using SBE-β-CD as crosslinking agent:

This procedure was selected to take advantage from the stabilizing properties of the CDs combined with the crosslinking ability toward CS and its derivatives showed by anionic CDs such as SBE-β-CD which has already been approved by FDA for pharmaceutical applications [41–43]. In this context, it should be also taken into account that the stabilizing effect exerted by CDs is dependent on their concentration, stability constant of the complex and drug degradation rate within the CD cavity.

Preliminarily, DA and SBE-β-CD were allowed to equilibrate in phosphate buffer (pH 2.7, 50 mM) under stirring at room temperature for 24 h, in order to minimize DA autoxidation. A DA/SBE-β-CD 3:1 molar ratio was chosen to obtain a high amount of the neurotransmitter in the complex. Afterward, DA (3.75 mg) was dissolved in 0.75 ml of CS- or GCS- or corresponding thiomers aqueous solution (0.20% w/v) in order to ensure a final concentration of 0.5% w/v and the resulting mixture was maintained under magnetic stirring for few min. Then, 0.24 ml of the previously prepared DA/SBE-β-CD mixture was added to the polycation solution, leading to NPs formation referred to as DA polycation/DA-CD.

Throughout the manuscript, NPs consisting of GCS and SBE-β-CD (without any DA) were denoted as GCS/CD NPs and they were achieved after the crosslinking of 0.75 ml of a GCS aqueous solution (0.20% w/v) by 0.24 ml of 0.45% w/v SBE-β-CD aqueous solution.

FITC labeled GCS based NPs encapsulating the neurotransmitter, denoted as DA FITC-GCS/DA-CD, were freshly prepared according to the procedure (c) and starting from FITC-GCS in turn prepared as reported in literature with slight modifications [44].

All the NPs prepared by each of the above reported methods were isolated by centrifugation (16,000*g*, 45 min,), re-suspended in ultrapure water by manual shaking and characterized for size, zeta potential, association efficiency (A.E.), neurotransmitter release and pH of the relative nanosuspension.

2.3. Physicochemical characterization of nanoparticles

For all tested NPs, mean diameters and polydispersity indexes (PI) were measured in double distilled water by photon correlation spectroscopy (PCS) using a Zetasizer NanoZS (ZEN 3600, Malvern, UK). The determination of the zeta-potential was carried out using laser Doppler anemometry (Zetasizer NanoZS, ZEN 3600, Malvern, UK) after dilution with 1 mM KCl and following a previously reported procedure [45].

2.4. High-performance liquid chromatography (HPLC) analysis

HPLC analyses of DA were carried out with an instrument constituted by a Waters Model 600 pump (Waters Corp., Milford, MA), a Waters 2996 photodiode array detector and a 20 μl loop injection autosampler (Waters 717 plus). Data were processed by the Empower™ Software Build. For analysis, the stationary phase was a Synergy Hydro-RP (25 cm × 4.6 mm, 4 μm particles; Phenomenex, Torrance, CA) column in conjunction with a pre-column C18 insert and the mobile phase was 0.020 M potassium phosphate buffer (pH 2.8) which eluted in isocratic mode at the flow rate of 0.9 ml/min. Standard calibration curves for DA determination were obtained at 280 nm wavelength dissolving DA in the eluent above mentioned and calibration curve linearity ($R^2 > 0.999$) was checked over the range of concentrations tested (4.75×10^{-4} to 1.5×10^{-5} M). The retention time of DA was 8 min.

2.5. Determination of DA association efficiency (A.E.)

The A.E. of DA/CS derivative-based NPs was obtained by an indirect method. All described particles were isolated from unbound DA by centrifugation (16,000*g*, 45 min, Eppendorf 5415D,

Eppendorf, Germany), and free DA in the supernatant was quantified by HPLC as described above. Experiments were performed in triplicate and the A.E. was calculated as follows (Eq. (1)):

$$\%\,\text{A.E.} = 100 \times (\text{Total DA} - \text{Free DA})/\text{Total DA} \quad (1)$$

2.6. Transmission electron microscopy (TEM) observations

The morphology of DA GCS/DA-CD NPs was examined by a transmission electron microscope (TEM, model JEM-1011, JEOL, Tokyo, Japan) operating at 80 kV. The sample was cast on carbon coated copper grid and negatively stained with a 2% (v/v) phosphotungstic acid solution for 30 s. The solvent was let to dry overnight at room temperature before the observation by TEM.

2.7. X-ray photoelectron spectroscopy (XPS) analysis for DA GCS/DA-CD nanoparticles

The surface of NPs formulations was analyzed to determine their chemical composition by XPS analysis. The different NPs formulations were placed as droplets on a gold sheet and, prior to the analysis, are allowed to dry at air. XPS measurements were carried out with a Thermo VG Thetaprobe spectrometer (Thermo Fisher Scientific, Inc., Waltham, MA, USA) using a microspot monochromatized Al Kα source (radiation line = 1486.6 eV). Fixed analyzer transmission (FAT) mode was employed both for survey scans (binding energy (BE) range 0–1200 eV, pass energy = 150 eV) and high resolution spectra (pass energy = 50 eV). Vacuum in the analysis chamber was maintained at 10^{-9} mbar. Data were processed using the Advantage software package. Sample charging effect on non-conductive surfaces was minimized by means of a low-energy flood gun. Charge referencing was done by setting the lower binding energy C1s photopeak at 285.0 eV (C1s aliphatic carbon). Quantification was performed by peak areas normalized by instrument manufacturer's acquisition parameters and sensitivity factors. Data were averaged over at least three points analyzed for each sample.

2.8. Interaction DA/SBE-β-CD assessed by nuclear magnetic resonance (NMR) spectroscopy

NMR experiments were performed at 25 °C on 1.76 mg/ml (1.55 mM) β-CD, 2.25 mg/ml (11.87 mM) DA and β-CD (3.97 mM)-DA (11.87 mM) mix in 100% D_2O, (pH 6.45). $^{1}H,^{13}C$HSQC spectra were acquired using a gradient-enhanced sequence in which coherence selection and water suppression were achieved by gradient pulses. Two transients were acquired over an F2 (^{1}H) spectral width of 10 ppm into 2048 complex data points for each of 256 t_1 increments with an F1 spectral width of 165 ppm centered at 75 ppm, with a delay $1/(8J_{CH})$ of 0.86 ms and a recycle delay of 1.0 s. The phase-sensitive ROESY spectrum was acquired with a spectral width of 10 ppm with 8 transients per increment for 256 t_1 increments into 2048 complex data points, a spin-lock time of 500 ms and a recycle delay of 2.0 s. All spectra were collected on a Bruker Avance 600 with an Ultra Shield Plus magnet using a triple-resonance probe equipped with *z* axis self-shielded gradient coils and processed using the standard Bruker software (TOPSPIN).

2.9. DA GCS/ DA-CD NPs formulation stability

To evaluate the stability of DA GCS/ DA-CD NPs both the particle size and the neurotransmitter autoxidation rate were considered. DA GCS/DA-CD NP water suspensions were maintained exposed to air at three different temperatures (4 °C, 25 °C and 37 °C) under agitation (100 rpm). Similarly, a DA water solution at pH 5 was treated for comparison. At several time points, NP size was measured by PCS and, moreover, the suspensions as well as the DA solution were monitored to detect when they turn pink and then replaced by a gray-black precipitate due to DA autoxidation [46]. Each experiment was performed in triplicate.

2.10. In vitro neurotransmitter release study from DA-loaded nanoparticles

To investigate batch-to-batch consistency, the *in vitro* DA release kinetics was evaluated according to our previously published protocol [47]. Briefly, freshly prepared DA-loaded NPs, corresponding to 70–200 μg of neurotransmitter, were suspended in 4.5 ml PBS (0.01 M, pH 7.4) and the dispersion was divided into 6 Eppendorf tubes, each one containing 750 μl of the medium. The tubes were then kept in a shaker at 37 °C at 100 rpm up to 6 h. At appropriate time intervals, these tubes were taken out from shaker and centrifuged at 16,000*g*, 45 min. The supernatant was analyzed for the DA content according to the HPLC protocol above reported.

The experiment for each type of NPs was performed in triplicates and results are expressed as means ± standard deviation.

2.11. Cell cultures of Olfactory Ensheathing Cells (OECs)

OECs were kindly obtained by Prof. R. Pellitteri Institute of Neurological Sciences—CNR—Section of Catania, Catania (Italy). OECs were isolated from 2-day-old rat pups (P2; Harlan) olfactory bulbs and cultured in DMEM/FBS supplemented with bovine pituitary extract, as previously described [48].

2.12. In vitro cytotoxicity studies of DA GCS/DA-CD NPs with OECs

OECs were plated at the number of 30,000 per each well of a 96-well plate. Cells were incubated with either DA GCS/DA CD NPs (200 μl, 50 μl, 12.5 μl, 3.12 μl, 0.78 μl of an initial stock solution of 75 μM) or GCS/CD NPs (200 μl, 50 μl, 12.5 μl, 3.12 μl, 0.78 μl) in complete medium. After 24 h, cells were tested for viability by the 3-(4,5-dimethylthiazol-2-yl)-2,5 diphenyl tetrazolium bromide (MTT) assay. Briefly, a stock solution of MTT (Sigma) in phosphate buffered saline (PBS) (5 mg/ml) was added to each well reaching a final concentration of 0.5 mg/ml (in 1000 μl of complete medium). After 4 h, the formazan crystals were dissolved in a 10% SDS/0.01 N HCl solution and measured spectrophotometrically by an ELISA reader (PowerWave HT, Bio-tek, Milan, Italy) at a wavelength of 570 nm with a reference wavelength of 690 nm. The relative viability was calculated in respect to control wells containing mock cells, *i.e.* cells treated with 150 mM NaCl (considered as 100%). 1% SDS-treated cells were used as positive control.

2.13. In vivo study with DA GCS/ DA-CD nanoparticles

2.13.1. Treatment schedule and HPLC analyses

Animals were briefly anesthetized with equithesin (3 ml/kg, i.p.) [Na-pentobarbital (0.972 g), chloral hydrate (4.251 g), magnesium sulfate (2.125 g), ethanol (12.5 ml), and propylene glycol (42.6 ml) in distilled water (total volume, 100 ml)] to ameliorate any suffering and intranasal delivery was carried out manually with the rat head in a supine position with the neck in extension. Freshly prepared DA GCS/DA-CD NPs at the dose of 10 mg/kg in 30 μl or, as a control, GCS/CD NPs (total volume of 30 μl) were delivered in the right nostril using an appropriate Eppendorf pipette, 5 μl at a time with a lapse of 2 min between each administration, for a total of 6 times. The left nostril was untreated to allow normal breathing. After administration, the rats were left in the same position until they recover from the anesthesia to

ensure that the fluid was completely inhaled. Then, rats were transferred to their home-cage. The successful nasal delivery by using this approach was confirmed by examination of fluorescence in the paraformaldehyde-perfused brains after nasal administration of DA FITC-GCS/DA-CD using the same approach (see below for details). For both treatment regimens, a dose of 10 mg/kg DA was given at each administration.

Rats were assigned to two experimental groups. The first group of rats was acutely treated with DA GCS/DA-CD NPs in the right nostril, while the left nostril was used as internal control. Thirty, 60 and 120 min after the intranasal administration the rats were sacrificed, and their brains were rapidly excised and freshly dissected to isolate separately the right (ipsilateral to the site of injection) and left (contralateral to the site of injection) striatum, which was flash frozen in dry ice, and stored at −80 °C for HPLC analyses at a later date. We have also collected the right and left striatum from naïve rats, which did not receive any treatment. The second group of rats was intranasally treated with DA GCS/DA-CD NPs or, GCS/CD NPs every other day for 14 days. Twenty-four h following the last administration, rats were sacrificed and right (ipsilateral) and left (contralateral) striatum was separately collected, and stored at −80 °C for HPLC analyses at a later date. As for the acute treatment, a naïve-group of animals was included. All striata were sonicated in ice-cold perchloric acid 0.1 M, centrifuged at 10,000*g* for 8 min at 4 °C and then supernatants were collected for NA, DA and DOPAC assay. The levels of monoamines and metabolite were quantified by HPLC coupled to an electrochemical amperometric detector, as previous reported [49].

2.13.2. Fluorescence microscopy on DA FITC-GCS/DA-CD nanoparticles

Freshly prepared DA FITC-GCS/DA-CD NPs were administered in the right nostril of rats as reported before. Animals were transcardially perfused with PBS followed by 4% paraformaldehyde (PFA)/PBS. The brain was removed from the skull, washed in PBS, post-fixed in 4% PFA/PBS for 24 h and then cryoprotected in 30% sucrose. Five µm-thick coronal sections of olfactory bulb were obtained on a sliding microtome adapted for cryosectioning. Sections were observed at Leica DM IRB microscope equipped with a JVC digital camera (FITC filter: excitation 395 nm; emission 509 nm).

2.14. Statistics

Data from different experimental groups were compared by a one-way analysis of variance (ANOVA) with $p < 0.05$ at 99% level of confidence (GraphPad Prism v. 4.00 GraphPad Software, Inc., San Diego, CA). Bonferroni posttests were used for post hoc contrast.

The striatal levels of NA, DA and DOPAC (pg/mg of wet tissue) were expressed as mean ± SEM. Within-group variability was analyzed through Levene test for homogeneity of variances. The data failed to meet the homoscedasticity assumption; therefore, they were analyzed by Mann–Whitney *U* test with Bonferroni's correction. DA turnover was expressed as DOPAC/DA ratio. The threshold for statistical significance was set at $p < 0.05$.

3. Results

3.1. Formulation and characterization of DA-loaded CS derivative-based NPs

Firstly, the experimental conditions allowing the preparation of CS derivative-based NPs in satisfactory way were explored. For this purpose, we used three approaches based on the ionic gelation method [41], a technique already carried out for preparing DA loaded CS based NPs [8]. The first approach (procedure a) consisted in dissolving the neurotransmitter in an aqueous acidic (AcOH 0.1% v/v) solution of CS derivative. The subsequent addition to the resulting mixture of TPP as polycation crosslinking agent yielded the corresponding nanocarriers. It should be noted that the neurotransmitter cannot be dissolved in the alkaline TPP solution because, in such conditions, it is very prone to autoxidation reactions [46]. However, according to the described procedure, negligible DA association efficiencies were observed (27% at most), not only for CS-based NPs but also for thiomer-based ones (Table 1) [8]. To increase the neurotransmitter loading, we subsequently evaluated the DA adsorption onto preformed unloaded CS derivative-based NPs (procedure b), similarly to that previously performed for CSNPs [8]. Generally, upon these conditions, greater association efficiencies were observed as reported in Table 1. Finally, a further procedure based on the use of the polyanionic SBE-β-CD as crosslinking agent in the ionic gelation process was taken into account [41]. More precisely, NPs were prepared by adding an acidic DA/SBE-β-CD mixture to the appropriate polycation solution containing further amount of neurotransmitter (procedure c). As shown in Table 1, with the latter procedure, the DA association efficiencies were in the range 27–54%.

In Table 1 the physicochemical properties of all the prepared NPs are also summarized. In general, it seems that NPs obtained following the methods (a) and (b) were quite bigger than those obtained by procedure (c) (*i.e.*, from 214 to >10^3 nm average particle size by procedures (a) and (b) compared with 326–598 nm by

Table 1
Physicochemical properties of DA loaded CS derivative-based NPs. PI: polydispersity index. A.E.: association efficiencies. Mean ± SD are reported, $n = 6$.

Formulation (pH nanosuspension)	Mean diameter (nm)	PI	Zeta potential (mV)	A.E. (%)
Procedure (a)				
DA in CSNAC/TPP	237 (±11)	0.49 (±0.1)	+20.3 (±0.5)	19.1 (±4.9)
DA in CSGSH/TPP	238 (±9)	0.48 (±0.2)	+25.6 (±0.8)	27.2 (±7.3)
DA in GCS/TPP	>1000	1		0
DA in GCSNAC/TPP	275 (±33)	0.43 (±0.01)	+18.1 (±0.2)	23.1 (±8.2)
Procedure (b)				
DA adsorbing CSNAC/TPP (pH 4.77)	487 (±26)	0.69 (±0.09)	+20.6 (±0.3)	20.3 (±3.2)
DA adsorbing CSGSH/TPP (pH 4.07)	214 (±7)	0.64 (±0.18)	+19.5 (±0.5)	24.8 (±4.0)
DA adsorbing GCS/TPP (pH 6.26)	291 (±44)	0.36 (±0.02)	+18.6 (±2.2)	78.0 (±1.7)
DA adsorbing GCSNAC/TPP (pH 4.61)	395 (±22)	0.51 (±0.01)	+20.0 (±0.6)	37.7 (±2.7)
Procedure (c)				
DA CS/DA-CD (pH 3.93)	497 (±21)	0.33 (±0.07)	+24.8 (±0.4)	27.8 (±6.4)
DA CSNAC/DA-CD (pH 3.07)	598 (±60)	0.35 (±0.04)	+26.9 (±0.5)	36.0 (±9.2)
DA CSGSH/DA-CD (pH 3.39)	521 (±16)	0.33 (±0.07)	+19.2 (±0.9)	27.1 (±4.9)
DA GCS/DA-CD (pH 5.7)	372 (±81)	0.26 (±0.07)	+9.3 (±1.3)	54.5 (±0.7)
DA GCSNAC/DA-CD (pH 3.49)	326 (±17)	0.35 (±0.03)	+20.4(±0.8)	27.2 (±5.8)

procedure (c)) (Table 1). However, besides an unsatisfactory A.E., the method (a) is also characterized by a broad distribution as proved by the PI values >0.43. Concerning the preparative method (b), despite a general greater A.E., even by this approach a broad particle distribution was observed (PI values in the range 0.35–0.69). Instead, a more homogeneous particle distribution was noted for NPs prepared following the procedure (c) (PI ranging from 0.26 to 0.35) even though, in this case intermediate association efficiencies were observed. Moreover, the particle size of GCS- and GCS-thiomers based NPs prepared following the procedure (c) was lower enough than the corresponding based on CS and CS-thiomers, despite the higher molecular weight of the former polycations.

For all tested particles, the zeta potential values were positive, varying between +18.1 mV and +25.6 mV for NPs prepared according to methods (a) and (b), while a wider range was observed for NPs prepared following the procedure (c) going from moderate (*i.e.*, +9.3 mV for DA GCS/DA-CD) to highly positive (+26.9 mV for DA CSNAC/DA-CD) values. Moreover, it was observed that the positive zeta potential values observed for GCS-based NPs prepared by this latter procedure were lower than those measured for the corresponding nanocarriers based on CS and CS-thiomers.

In view of an application of these formulations for nasal administration, the pH of each nanosuspension was assessed. As shown in Table 1, the pH values observed were in the range from 3.49 to 6.26. In this regard, taking into account the prevention of the nasal mucosa irritation as well as the normal pH value of the nasal cavity (*i.e.*, 5.5–6.0 [28,29]), the pH value of the DA GCS/DA-CD NPs fell in the optimal range therefore, for the following studies, our attention has been focused on this formulation.

According to the TEM observations (Fig. 1), it appears that DA GCS/DA-CD NPs are composed of slightly lengthened spheroidal although particle size arising from TEM was slightly lower than that determined by PCS.

3.2. Interaction DA-SBE-β-CD assessed by NMR spectroscopy

In order to investigate the inclusion mode of DA, we initially used unsubstituted β-CD and applied heteronuclear NMR spectroscopy. Proton chemical shift data of DA in the free state and in complex with β-CD are shown in Table 2. $^{1}H–^{13}C$ HSQC experiments showed that the largest proton chemical shift changes of β-CD upon complex formation (Fig. 2) were exhibited by H3′, H5′, and H6′, at one edge of the CD molecule, with upfield shifts of 0.049, 0.075 ppm, and 0.027 ppm, respectively (Table 2). On the other hand, all protons of the DA molecule exhibited small but measurable chemical shift changes upon complex formation (Fig. 3). In order to identify proton–proton dipolar connectivities, rotating frame NOE experiments (ROE) were used. In fact, among the different NMR experimental approaches, the ROESY experiments are particularly suitable for the structure determination of molecular complexes [50].

Table 2
Proton chemical shift data (ppm) of β-CD and DA in the free state and in the complex with DA and β-CD, respectively. $\Delta\delta = \delta_{complex} - \delta_{free}$ (in ppm).

β-CD proton	δ_{free}	$\delta_{complex}$	$\Delta\delta$	DA proton	δ_{free}	$\delta_{complex}$	$\Delta\delta$
H1′	5.007	4.994	−0.013	H3	6.831	6.817	−0.014
H2′	3.589	3.587	−0.002	H4	6.685	6.672	−0.013
H3′	3.902	3.853	−0.049	H6	6.774	6.763	−0.011
H4′	3.523	3.518	−0.005	H9	3.154	3.144	−0.010
H5′	3.806	3.731	−0.075	H10	2.806	2.807	0.001
H6′	3.815	3.788	−0.027				

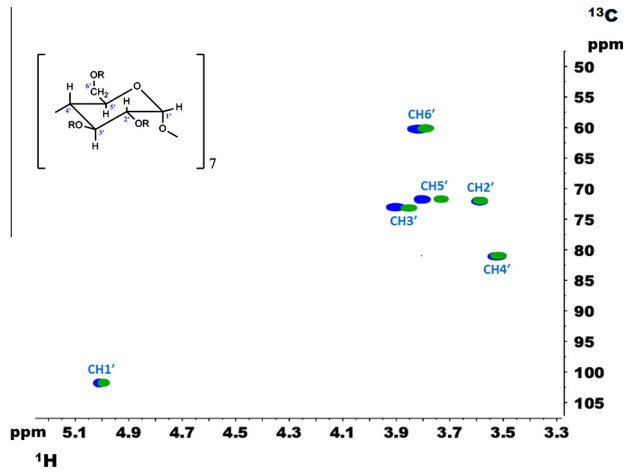

Fig. 2. Overlay of $^{1}H–^{13}C$ HSQC spectra collected at 25 °C on 1.76 mg/ml (1.55 mM) β-CD solution (blue contours), and β-CD (3.97 mM)-DA (11.87 mM) mix (green contours) in 100% D_2O (pH 6.45). (For interpretation of the references to color in this figure legend, the reader is referred to the web version of this article.)

Specifically, two-dimensional ROESY experiments were used to estimate the inclusion structure of the β-CD-DA complex. Analysis of the ROESY spectrum of the β-CD-DA mix (Fig. S1 Appendix), allowed us to identify some intermolecular cross-peaks between the β-CD and the DA protons. Fig. 4 shows two enlarged regions of the ROESY spectrum. The H9 and H10 protons of DA displayed a cross-peak with the H3′ proton of β-CD, the H4 and H6 protons of the guest molecule gave a cross-peak with both the H3′ and H5′ protons of the host, the H3 protons of the DA gave a cross-peak with both H5′ and H6′ protons of β-CD, while only the H4 proton of DA showed a cross-peak with the H2′ proton of β-CD.

Taking into account that the strength of the ROE signal is proportional to the distance between the atom pair, the ROEs were interpreted in a semi-quantitative way and converted into three classes of distance restraints (strong, medium, or weak), considering the average intensity plus or minus 0.5 standard deviation. The DA-β-CD intermolecular ROEs are listed in Table 3.

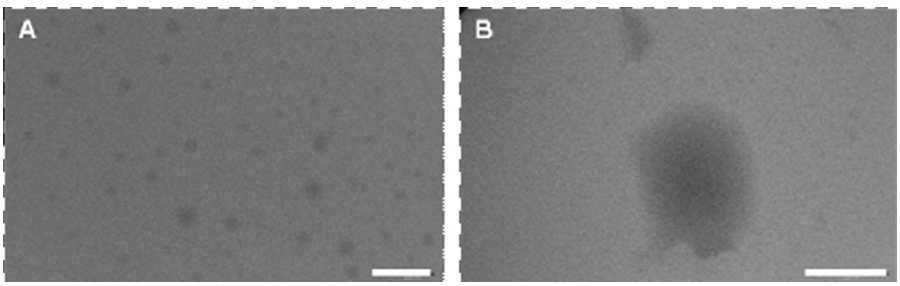

Fig. 1. TEM micrographs of DA GCS/DA-CD NPs (A, bar 500 nm; B, bar 200 nm).

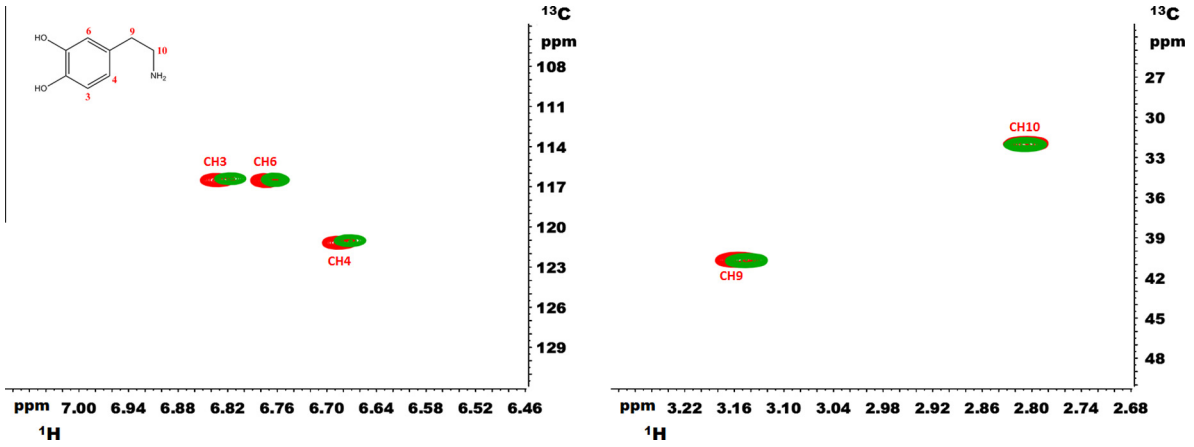

Fig. 3. Overlay of two different regions of the ^{1}H–^{13}C HSQC spectra collected at 25 °C on 2.25 mg/ml (11.87 mM) DA solution (red contours) and β-CD (3.97 mM)-DA (11.87 mM) mix (green contours) in 100% D_2O (pH 6.45). (For interpretation of the references to color in this figure legend, the reader is referred to the web version of this article.)

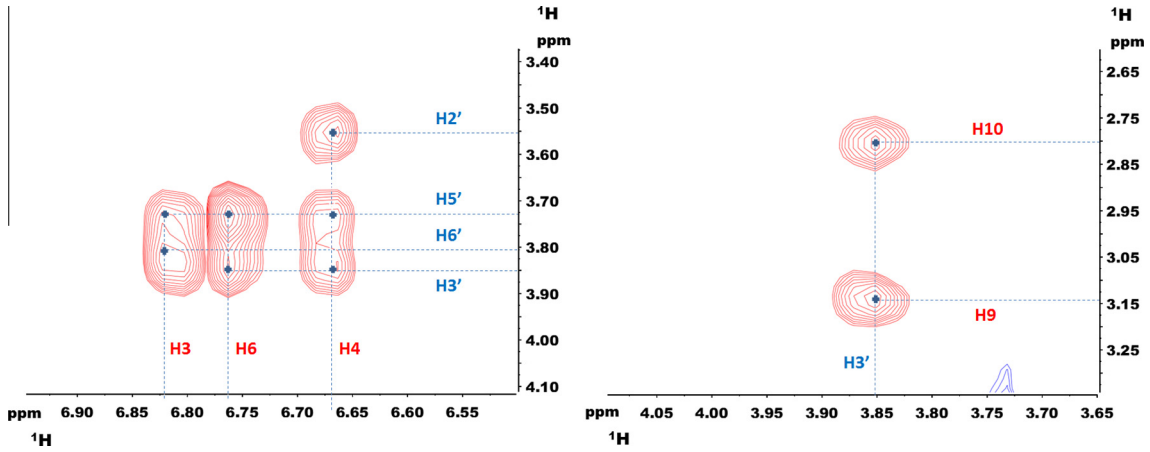

Fig. 4. Partial contour plots of the ROESY spectrum of the β-CD (3.97 mM)-DA (11.87 mM) mix in 100% D_2O at 25 °C.

Table 3
DA-β-CD intermolecular ROEs. The intensity range is obtained by integration of cross-peaks in the ROESY spectrum.

β-CD proton	DA proton	ROE
H5′	H6	Strong
H6′	H3	Medium
H3′	H6	Medium
H3′	H9	Medium
H2′	H4	Medium
H5′	H3	Medium
H3′	H10	Medium
H3′	H4	Weak
H5′	H4	Weak

The NMR analysis was also performed on the DA complex with sulfobutylether-β-cyclodextrin. Notably, ^{1}H–^{13}C HSQC spectra showed no chemical shift variation for the sulfobutylether substituents (H8′, H9′ and H10′) upon complex formation with DA, while the group of signals ascribable to H3′, H5′ and H6′ experience the largest proton chemical shift changes (Fig. S2 Appendix). Such signals were partially overlapped and poorly distinguishable due to the partial degree of substitution, that prevented any unambiguous cross-peak identification. On the other hand, the DA molecule exhibited similar chemical shift changes as those observed with unsubstituted β-CD (Fig. S3 Appendix). Moreover, the ROESY experiment confirmed that the signals affected by intermolecular interactions were the same for the complexation of DA in SBE-β-CD or unsubstituted β-CD (Fig. S4 Appendix).

3.3. DA location on DA GCS/DA-CD formulation determined by XPS

XPS was employed to investigate the surface chemical composition of pure and DA GCS/DA-CD and, in particular, to ascertain the DA localization on the NPs. The atomic percentages of all the analyzed samples (*i.e.*, the starting materials and the nanoparticle systems) are summarized in Table 4.

The main elements detected on GCS surfaces were carbon, oxygen and nitrogen, while the other ones were residuals arising from the preparation media. Similar elements were detected on the SBE-β-CD sample, with the additional sulfur presence and the absence of nitrogen, according to the chemical structure.

In the case of the DA GCS/DA-CD NPs, since DA did not introduce peculiar signals to the XPS spectra but simply adds contributions to carbon, nitrogen and oxygen spectral regions, the presence of DA on the nanoparticles surface could be assessed only by an accurate signal curve-fitting. The N1s XPS regions was chosen for this purpose. N1s spectra of pure DA, pure GCS, GCS/CD NPs and DA GCS/DA-CD NPs are reported in Fig. 5, while peaks assignments, BE values and relevant atomic percentages are summarized in Table 5.

Table 4
Surface composition (*i.e.*, atomic percentages obtained by XPS analysis) of the starting materials (*i.e.*, GCS, SBE-β-CD and DA) and the nanoparticle systems (*i.e.*, GCS/CD NPs and DA GCS/DA-CD NPs).

Element	Atomic percentage (%)				
	GCS	SBE-β-CD	DA	GCS/CD NPs	DA GCS/DA-CD NPs
C1s	61 ± 5	55.1 ± 1.1	69.9 ± 1.4	61.0 ± 1.0	58 ± 2
O1s	19.3 ± 0.3	34.2 ± 1.2	16.7 ± 0.5	33.0 ± 0.5	28.7 ± 1.6
N1s	2.1 ± 0.2	–	6.4 ± 0.7	4.1 ± 0.2	3.64 ± 0.14
S2p	–	3.75 ± 0.18	–	1.9 ± 0.2	1.7 ± 0.4
Cl2p	7 ± 3	–	7.0 ± 0.2	–	2.43 ± 0.18
K2p	5.4 ± 1.8	–	–	–	
Na1s	5.2 ± 0.6	3.6 ± 0.4		–	2.53 ± 0.14
P2p	–	3.3 ± 0.5	–	–	2.9 ± 0.4

The N1s spectrum of pure GCS sample (Fig. 5a) showed, as expected, only aminic nitrogen (399.7 eV). On the other hand, only one component at 402.0 eV, attributable to quaternary nitrogen, was detected in DA XPS spectrum (Fig. 5b).

The N1s signal of DA GCS/DA-CD NPs (Fig. 5c) could be curve-fitted by two peaks: aminic and quaternary nitrogen functionalities, present in an almost similar amount. The quaternary nitrogen species induce an ionic interaction with the $-SO_3^-$ groups relevant to SBE-β-CD. This interaction could justify the shift of the S2p signal BE in the NPs samples with respect to the same signal in pure SBE-β-CD, *i.e.*, 168.9 eV versus 168.1 eV, respectively (data not shown). Fig. 5d shows that the percentage of the DA contribution at 402.0 eV significantly increased with respect to that observed on GCS/CD NPs, reaching the atomic percentage of about 77%, although the aminic component remained still evident.

3.4. DA GCS/ DA-CD NPs formulation stability

As already observed for DA adsorbed on CS-based NPs [8], increase of DA GCS/DA-CD NP size and polydispersity index was detected at all the three temperatures investigated and, as expected, this effect was faster at the highest temperature (*i.e.*, 37 °C). Thus, while at 4 °C the average particle size was greater than 700 nm after 12 h, the aggregate formation at 37 °C occurred after 6 h. However, it was interesting to note that the formation of the gray-black precipitate, indicative of the neurotransmitter autoxidation, occurred after 72 h at 37 °C while, at the same temperature, the DA control solution (pH 5) turned pink after 16 h and the gray–black precipitate was detected after 48 h. These results suggested that the nanocapsulation, could slow the rate of the neurotransmitter autoxidation process.

3.5. DA release kinetics from nanocarriers

The *in vitro* release kinetics of NPs were determined in PBS (pH 7.4) without enzymes and some marked differences were observed between the DA adsorbing nanocarriers and those prepared using SBE-β-CD as crosslinking agent. While the DA adsorbing NPs showed a release profile endowed with an immediate burst effect, this last was less evident in NPs prepared using SBE-β-CD. For instance, as shown in Fig. 6, while DA adsorbing GCSNAC/TPP NPs exhibited a prompt release of about 30% of neurotransmitter within 1 h, the same release was observed with DA GCS/DA-CD NPs after 3 h.

3.6. In vitro cytotoxicity of loaded and unloaded GCS NPs

In order to see whether particles were toxic in their way to the olfactory bulb, GCS NPs either loaded with DA or unloaded were incubated with OECs and cell viability was assessed after 24 h by the MTT assay. As shown in Fig. 7, unloaded GCS NPs were not toxic to OECs at any concentration tested, whereas exposure of OECs to DA GCS/DA CD for 24 h resulted in a dose-dependent reduction of viability.

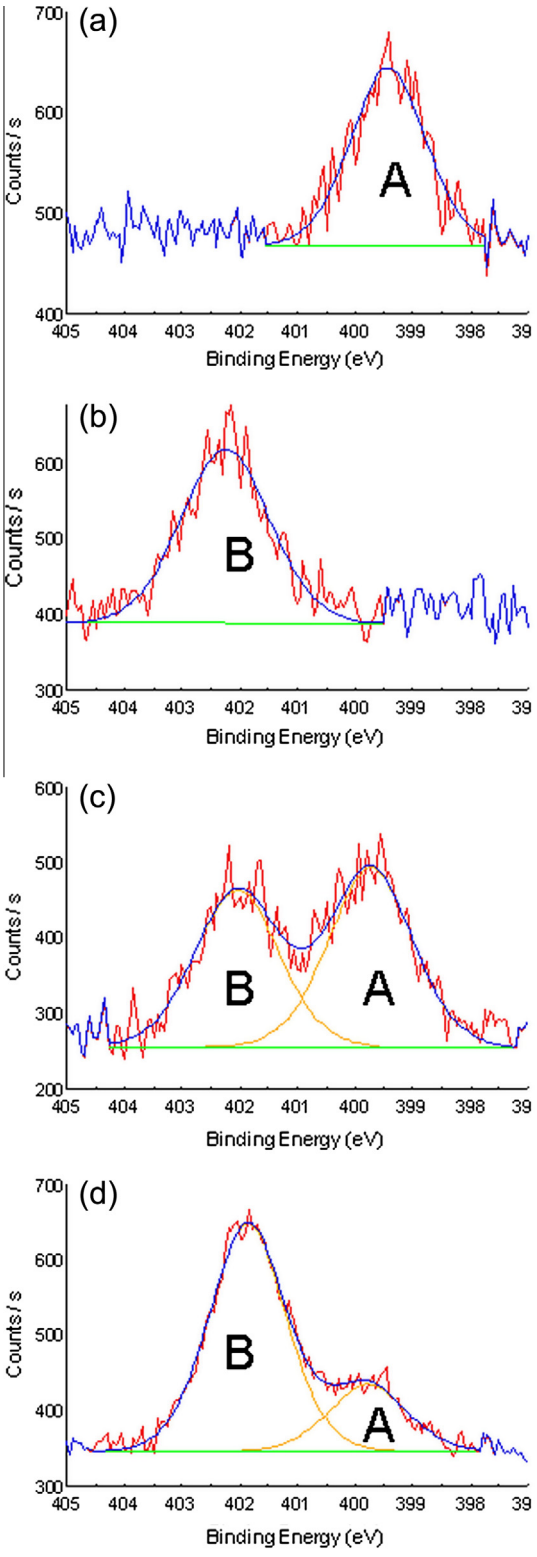

Fig. 5. High resolution spectra of N1s region relevant to (a) pure GCS, (b) pure DA, (c) GCS/CD NPs and (d) DA GCS/DA-CD NPs.

Table 5
Peak position and relative abundance of the N1s peak components relevant to GCS, DA, GCS/CD NPs and DA GCS/DA-CD NPs displayed in Fig. 6. The maximum error on the peak position is ±0.2 eV.

Attribution	BE (eV)	Atomic percentage (%)			
		GCS	DA	GCS/CD NPs	DA GCS/DA-CD NPs
A: N–H	399.7	100	–	53.7	22.8
B: $^{+}$N–H	402.0	–	100	46.3	77.2

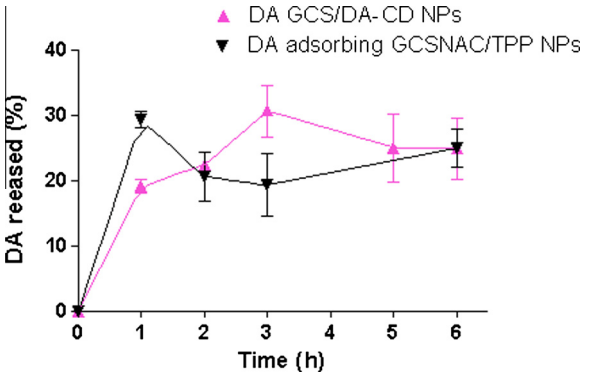

Fig. 6. *In vitro* release profiles of DA adsorbing GCSNAC/TPP NPs and DA GCS/DA-CD NPs in PBS (pH 7.4).

3.7. Biodistribution study of DA FITC-GCS/DA-CD investigated by fluorescence analysis

To determine whether particles reached the olfactory bulb upon the nasal route, DA FITC-GCS/DA-CD formulation was administered in the right nostril and fluorescence microscopy analysis was performed at several time-points, ranging from 20 to 150 min, after administration. No specific signals were observed at earlier time-points, whereas the green fluorescence associated to DA FITC-GCS/DA-CD was observed at 150 min only in the right olfactory bulb ipsilateral to the site of administration without any evident morphological tissue damage, as determined by visual inspection (Fig. 8).

3.8. Effects of intranasal DA GCS/DA-CD administration on striatal DA, DOPAC and NA level

Statistical analysis showed that the acute administration of DA GCS/DA-CD into the right nostril did not modify the levels of DA, DOPAC and NA in either right or left striatum at selected time points postadministration (30, 60 and 120 min). Moreover, monoamine levels in the DA GCS/DA-CD treated-rats were not statistically different from those found in naïve rats (Table 6).

On the contrary, repeated intranasal administration of DA GCS/DA-CD into the right nostril elicited a significant DA increase in the right striatum compared to the contralateral striatum (+46%, $p = 0.0022$), whereas no difference was found with the striatal DA level in the GCS/CD NPs-treated rats. Moreover, the DA level in the right striatum of DA GCS/DA-CD treated-rats was significantly higher compared to the DA in the right striatum of GCS/CD NPs treated-rats (+40%, $p = 0.0043$) (Fig. 9, panel A). No differences were observed in the DOPAC level and DA turnover (DOPAC/DA ratio) across the two striata of either DA GCS/DA-CD-treated or GCS/CD NPs-treated-rats (Fig. 9, panel B and C). Likewise, neither DA GCS/DA-CD nor GCS/CD NPs treatment had any significant effect on striatal NA level across the two hemispheres, although we observed a trend toward an increase of NA level in the right striatum of DA GCS/DA-CD-treated rats compared to the contralateral striatum (+38%, n.s.) (Fig. 9, panel D).

4. Discussion

The development of therapeutic strategies focused not only at addressing the motor symptoms of PD but also at modifying both the course of the disease and the neurodegenerative process still constitutes an unresolved challenge for the scientific community involved in this field [4,51]. To face this issue, new drug targets and appropriate delivery systems as well are needed to overcome

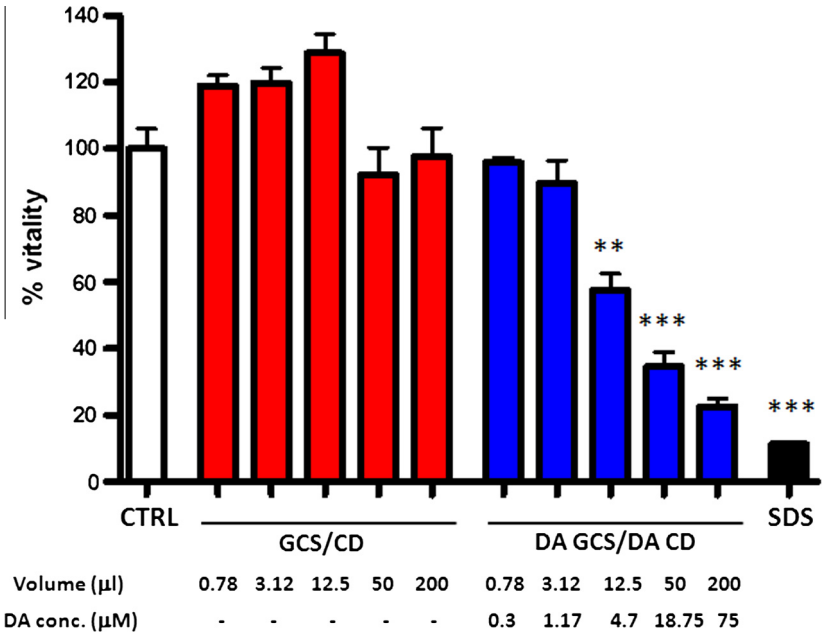

Fig. 7. Cytotoxicity of DA GCS/DA-CD and GCS/CD. OECs were challenged with DA GCS/DA-CD for 24 h at the indicated volumes and DA concentrations. GCS/CD NPs were used at equivalent volumes. Cells were then assayed for vitality by the MTT assay. Control (CTRL) cells are untreated cells (100% of vitality), whereas SDS denotes positive controls. $^{**}p < 0.01$ versus CTRL; $^{***}p < 0.0001$ versus CTRL. Data are expressed as average ± SD of two experiments carried out each in duplicate.

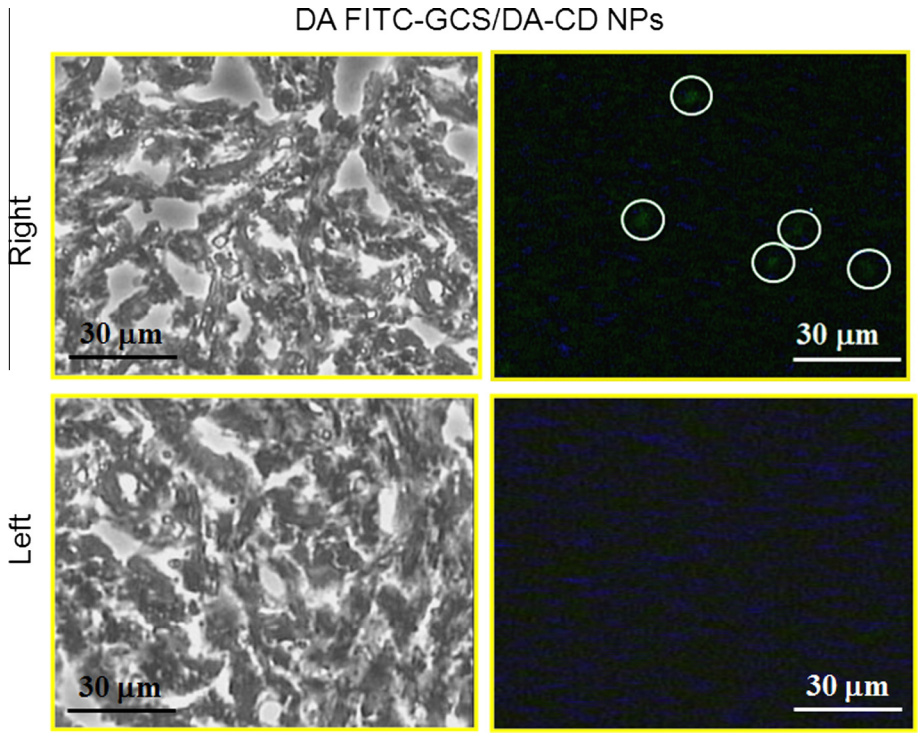

Fig. 8. Biodistribution of DA FITC-GCS/DA-CD at 150 min in right and left olfactory bulb section after administration in the right nostril. Left panels: representative bright fields; right panels: epifluorescence of the same fields. White circles highlight green DA FITC-GCS/DA-CD. Original magnification 20×. (For interpretation of the references to color in this figure legend, the reader is referred to the web version of this article.)

Table 6
Monoamines level (pg/mg of wet tissue) in the striatum of naïve rats and effect of single administration in the right nostril of DA GCS/DA-CD NPs on the DA, DOPAC and NA level in the right and left striatum of rats.

		Naïve	DA GCS/DA-CD NPs administered into the right nostril		
			30 min	60 min	120 min
DA	Left	1932 ± 210	2224 ± 27	2288 ± 318	1605 ± 558
	Right	2386 ± 310	2190 ± 73	1826 ± 304	1838 ± 230
DOPAC	Left	849 ± 288	1093 ± 155	994 ± 87	957 ± 125
	Right	915 ± 325	1077 ± 441	765 ± 162	708 ± 134
NA	Left	58 ± 28	71 ± 3	60 ± 15	56 ± 22
	Right	61 ± 19	68 ± 8	55 ± 16	43 ± 18

Data are expressed as mean ± S.E.M. of $n = 6$ animals per group. Statistical analysis (Mann–Whitney U test) showed no statistical significance ($p > 0.05$).

the formidable obstacle represented by the BBB that limits the distribution of drugs from blood to brain. In this context, in the last decade an increasing interest has been raised toward nanocarriers, including polymeric- and lipid-nanoparticles, able to improve the brain delivery of CNS therapeutic agents [4]. In addition, ever growing attention has been focused to the intranasal administration route because it constitutes a non invasive method to bypass the BBB, enabling the delivery of both small- and macro-molecules to the CNS [6]. With respect to the PD treatment, actually nanocarriers loaded with L-Dopa or DA receptor agonists for systemic direct nose-to-brain delivery have previously been evaluated using CS NPs [4,52]. Instead, the intranasal delivery of DA-loaded NPs has not been previously evaluated. Therefore, the aim of the present work was to gain information on the potential of CS-, CGS- and corresponding thiomer-based NPs as nanocarriers for delivering the neurotransmitter to the brain following a nasal administration as a new strategy for PD treatment. An initial issue was to find an efficient preparative method for satisfying two important requirements, *i.e.*, to avoid both irritation of the nasal mucosa and the autoxidation of the neurotransmitter. At first, the classic ionic gelation method employing TPP as crosslinking agent and dissolving DA in the polycation containing solution was followed. However, in this way disappointing results were obtained. The adsorption of DA on preformed unloaded CS- and derivative-based NPs improved the neurotransmitter loading but the pH of this nanosuspensions was out of the optimal range for a safe intranasal administration. In addition, it should be also taken into account that, as previously observed [8], from these DA surface adsorbing nanocarriers, the neurotransmitter is promptly released (burst effect) and it may be potentially dangerous since a nonphysiological stimulation of striatal DA receptors may occur. Better results were observed using the anionic SBE-β-CD as crosslinking agent of the polycations. Following this procedure, the particle size of the GCS-based NPs resulted quite lower than the corresponding CS-based NPs, despite the molecular weight of the former polymer was bigger (400 kDa and 110 kDa, respectively). Moreover, CS-based NPs showed positive zeta potential values higher than those measured for GCS-based NPs. These results, taken together, may suggest a more external location of DA for the latter particles which may shield the inherent positive charge and may bring about conformational modifications of the polycations (GCS and GCS-NAC), leading to NPs with a more compact structure.

The discrepancy between the particle size determined by TEM and that measured by PCS constitutes an outcome which has been often previously observed. It can be rationalized by the dehydration process of NPs occurring in sample preparation or taking into account that by PCS a hydrodynamic radius is measured with an overestimation of the NPs size [53].

As above indicated, the main reason for which our attention was focused to the nanocarrier DA GCS/DA-CD was that the observed pH value (5.7) was just inside the optimal range.

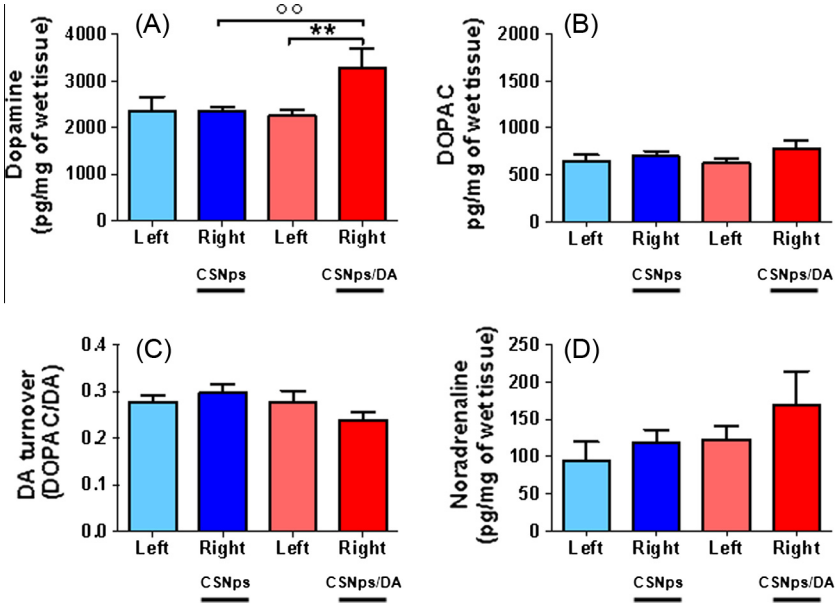

Fig. 9. Effect of repeated injections in the right nostril of either DA GCS/DA-CD NPs or GCS/CD NPs on DA (A), DOPAC (B), DA turnover (C) and NA (D) level in the right and left striatum of rats. Data are expressed as mean ± S.E.M. of $n = 6$ animals per group. Mann Whitney test with Bonferroni's correction. $^{**}p < 0.01$ versus contralateral striatum of DA GCS/DA-CD NPs-treated rats; $^{\circ\circ}p < 0.01$ versus right striatum of GCS/CD NPs-treated rats.

However, additional reasons that made this formulation attractive were the presence of both a cyclodextrin (SBE-β-CD) with potential DA stabilizing ability and a polymer (GCS) with mucoadhesive and P-gp/MDR1 inhibition properties [36].

To elucidate the type of interaction between DA and SBE-β-CD, an NMR study was carried out. CDs have an overall shape reminiscent of a truncated cone with an internal cavity, which is predominantly hydrophobic [54]. The internal cavity is open at the two ends, which have different diameters and are therefore referred to as the wide and narrow rings. Protons H3′ and H5′ from each sugar unit face the internal cavity and they are located near the wide and narrow ring, respectively. They can be used therefore to probe the internal cavity of CDs for the presence of a guest molecule and to understand the nature of this interaction [55,56].

Considering that NMR experiments highlighted a similar inclusion mode of DA in β-CD or SBE-β-CD, we can delineate the DA orientation within the SBE-β-CD cavity, using the results obtained with unsubstituted β-CD samples. $^{1}H–^{13}C$ HSQC experiments indicated that H3′, H5′ and H6′ of β-CD experienced the largest proton chemical shift changes upon complex formation, while the DA molecule exhibited small chemical shift changes at positions 3, 4, 6 and 9. The results were consistent with a β-CD-DA complex where DA occupied the cavity of the truncated cone β-CD. Moreover, the ROESY experiment allowed to define the orientation of the DA molecule within the β-CD cavity. The intermolecular cross-peak analysis deduced from ROESY cross-peak intensity suggested that the OH groups of the DA molecule were close to the narrow rim of the cavity whereas the NH_2 group lies on the wider rim of β-CD as graphically reported in Fig. 10. These results, taken together, suggested that the role of SBE-β-CD in preparing DA polycation/DA-CD NPs was not only to crosslink the polycation but also to form an inclusion complex with the neurotransmitter. It is reasonable to suppose that this complex, in some extent, may limit its autoxidation reaction.

XPS analysis of the DA GCS/DA-CD NPs provided a clear evidence of the presence of DA on the NPs surface, although the contribution of the nanosystem matrix was still observed. On the other hand, comparing the XPS results with those obtained when DA was

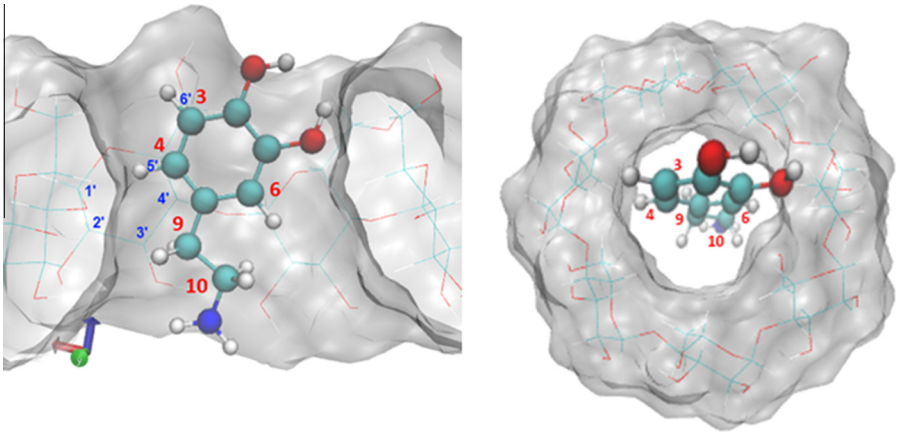

Fig. 10. Longitudinal cross-section (left) and orthogonal top view (right) of the β-CD-DA complex. The DA moiety is displayed in ball and stick and the β-CD molecules as wireframe with semi-transparent molecular surface.

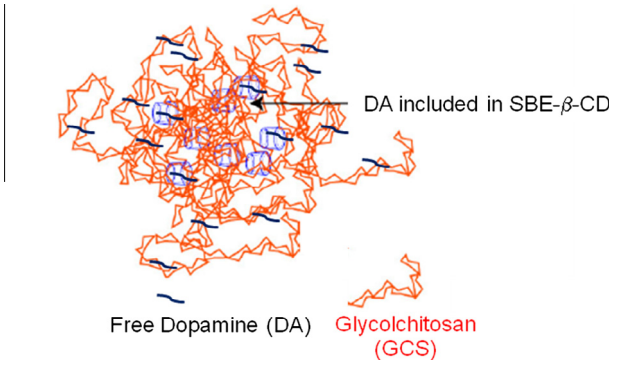

Fig. 11. Schematic representation of the DA GCS/DA-CD NPs structure (adapted from Ref. [29] with permission).

adsorbed on chitosan-based NPs [8] an interesting conclusion may be drawn. Actually, in the latter formulation, the only contribution of the neurotransmitter appeared in the N1s region, suggesting that most of DA was adsorbed on the chitosan NPs surface. As for DA GCS/DA-CD NPs besides the surface localization of DA on the outer surface of the NPs, the presence of the neurotransmitter in the NPs inner matrix layers cannot be excluded. In Fig. 11, a schematic representation of the structure of these carriers is shown.

This outcome is also in good agreement with the *in vitro* release kinetic studies from nanocarriers that, although are depending on several factors such as the amount of crosslinking agent, showed a faster neurotransmitter release from DA adsorbing NPs such as GCSNAC/TPP NPs compared to that from DA GCS/DA-CD NPs. It should be noted that the release kinetics were followed up to 6 h because after this time the autoxidation of the neurotransmitter [8,46] begins leading to increasing gray to black precipitate formation of melanin compounds. In this regard, the delayed formation of the gray–black precipitate observed with DA GCS/DA-CD NPs compared to the control (*i.e.*, DA solution) clearly suggested a stabilizing effect due to the nanocapsulation, very probably consequent to the inclusion in the SBE-β-CD cavity.

Although it was also expected that the *in vivo* release features could even markedly change from those observed *in vitro*, the *in vivo* studies were performed using only freshly prepared samples in order to limit the effects of DA chemical instability.

Exposure of primary OECs to DA-loaded GCS/CD nanoparticles resulted in a dose-dependent reduction of viability, whereas unloaded GCS/CD NPs demonstrated to have an excellent biocompatibility profile. DA caused cell death of OECs at concentrations lower than those previously reported by others to be neurotoxic to cortical and striatal neurons [57], indicating that neuronal cell types might be differently responsive to DA. Although we do not know the mechanism of toxic action of DA on OECs, we observed that after 24 h of incubation some products of oxidation appeared. This may be in agreement with previous studies reporting the generation of toxic metabolites by DA autoxidation or through the action of monoamine oxidase, a mitochondrial enzyme. DA autoxidation leads to the production of toxic oxygen radicals and quinines causing neurodegeneration associated with oxidative stress [58–60]. However, a correlation between the *in vitro* results to the *in vivo* studies is not simple, principally because no gross tissue damage was observed in the olfactory bulb of rats administered with DA GCS/DA CD (Fig. 8).

Moreover, we performed the *in vivo* studies to assess whether the intranasal administration of DA-loaded CS derivative-based NPs could influence the monoamine content in the striatum, which is the main target region for symptomatic treatment of PD and it is known to be rich in dopaminergic nerve terminals. To this aim, rats were administered with a single or repeated drug regimen only in one nostril (the right nostril was arbitrarily chosen). The left nostril/hemisphere was used as internal control allowing us to significantly reduce the number of animals used in the study, as recommended by the guidelines for the ethical use of animals in research.

Nose-to-brain delivery characteristic of nanoparticles was investigated by *ex vivo* fluorescence imaging technique using FITC as a tracer. The image of DA FITC-GCS/DA-CD NPs administered into the right nostril showed that fluorescence diffused from the right nostril only to the ipsilateral olfactory bulb. To this regard, it has been demonstrated that the olfactory epithelium projects mainly to the ipsilateral hemisphere and that drugs uptake from the nasal mucosa epithelium can achieve the brain via a direct pathway mainly along the olfactory nerve by passing the BBB [61,62].

After single administration we did not observe any changes in the striatal level of monoamines, therefore, we increased the number of administration to balance out the limited single administered dose caused by the small volume of the nasal cavity. After repeated administration we found a significant increase in striatal DA levels just in the right striatum (ipsilaterally to the site of administration) without any changes in the DOPAC and DA turnover. Likewise, striatal NA level across the two hemispheres was unaffected by treatments. de Souza Silva et al. [11] have previously shown that bilateral intranasal DA administration resulted in significantly increased DA levels in the neostriatum and nucleus accumbens immediately after administration. The discrepancy between de Souza Silva's and our study might be attributed to the differences in the experimental protocols (unilateral versus bilateral administration of drug into the nostrils) and mostly due to the use of microdialysis versus tissue content analysis.

5. Conclusions

DA GCS/DA-CD appears as a promising nanocarrier for non-invasive delivery of DA to the striatum by nasal route. This nanosystem is based on the interesting biomaterial GCS 400 kDa combined with the cross-linking and DA inclusion capabilities of SBE-β-CD. It seems that the location of the neurotransmitter is both on the surface and inside the nanosystem matrix. This feature may provide a more controlled *in vivo* release leading to a more physiological stimulation of striatal DA receptors. This study may represent a starting point of a new approach for the PD treatment different from that conventional based on L-Dopa administration.

Acknowledgments

This work was supported by grants from MIUR (Ministero dell'Istruzione, dell'Università e della Ricerca), Progetto PRIN 2010–2011 2010H834LS_005 to A.T., G.T., M.C., and G.P., as well as Progetto PRIN 2010–2011 20109PLMH2 to S.D.G, and FIRB 2011—Rete Integrata per la Nano Medicina, RBAP114AMK to V.M., and F.A.

TEM and particle size of NPs were partially supported by Sens&Micro LAB Project (2007–2013) funded by Apulia Region (Italy) and PONa300369 "Laboratorio per lo Sviluppo Integrato delle Scienze e delle Tecnologie dei Materiali Avanzati e per dispositive innovativi-LABORATORIO SISTEMA" financed by the Italian MIUR (Ministero dell'Istruzione, dell'Università e della Ricerca), respectively. Thanks are due to Dr. R. Comparelli (CNR-IPCF, Bari) for his help with TEM analysis, to Prof. R. Pellitteri (University of Catania, Italy) for providing us the Olfactory Ensheathing Cells and to Dr. Sara Cannito for her help with *in vivo* studies and the Consorzio Interuniversitario di Ricerca in Chimica dei Metalli nei Sistemi Biologici (CIRCMSB).

Appendix A. Supplementary material

Supplementary data associated with this article can be found, in the online version, at http://dx.doi.org/10.1016/j.ejpb.2015.05.019.

References

[1] J.A. Obeso, M.C. Rodríguez-Oroz, B. Benitez-Temino, F.J. Blesa, J. Guridi, C. Marin, M. Rodriguez, Functional organization of the basal ganglia: therapeutic implications for Parkinson's disease, Mov. Disord. 23 (Suppl. 3) (2008) S548–559.

[2] A. Di Stefano, P. Sozio, A. Iannitelli, L.S. Cerasa, New drug delivery strategy for improved Parkinson's disease therapy, Expert Opin. Drug Delivery 6 (2009) 389–404.

[3] I. Aviles-Olmos, Z. Kefalopoulou, T. Foltynie, Understanding and prevention of "therapy-induced" dyskinesias, Parkinsons Dis. 2012 (2012) 640815, http://dx.doi.org/10.1155/2012/640815.

[4] E. Garbayo, E. Ansorena, M.J. Blanco-Prieto, Drug development in Parkinson's disease: from emerging molecules to innovative drug delivery systems, Maturitas 76 (3) (2013) 272–278.

[5] N.V. Chemuturi, J.E. Haraldsson, T. Prisinzano, M. Donovan, Role of dopamine transporter (DAT) in dopamine transport across the nasal mucosa, Life Sci. 79 (2006) 1391–1398.

[6] J.J. Lochhead, R.G. Thorne, Intranasal delivery of biologics to the central nervous system, Adv. Drug Delivery Rev. 64 (7) (2012) 614–628.

[7] L. Montenegro, A. Trapani, C. Carbone, A. Latrofa, G. Puglisi, In vitro evaluation on a model of blood brain barrier of idebenone-loaded solid lipid nanoparticles, J. Nanosci. Nanotechnol. 12 (2012) 330–337.

[8] A. Trapani, E. De Giglio, D. Cafagna, N. Denora, G. Agrimi, T. Cassano, S. Gaetani, V. Cuomo, G. Trapani, Characterization and evaluation of chitosan nanoparticles for dopamine brain delivery, Int. J. Pharm. 419 (2011) 296–307.

[9] M.A. de Souza Silva, C. Mattern, R. Hacker, P.J. Nogueira, J.P. Huston, R.K.W. Schwarting, Intranasal administration of the dopaminergic agonists L-DOPA amphetamine and cocaine increases dopamine activity in the neostriatum: a microdialysis study in the rat, J. Neurochem. 68 (1) (1997) 233–239.

[10] M.A. de Souza Silva, C. Mattern, R. Hacker, C. Tomaz, J.P. Huston, R.K.W. Schwarting, Increased neostriatal dopamine activity after intraperitoneal or intranasal administration of L-DOPA on the role of benserazide pretreatment, Synapse 27 (1997) 294–302.

[11] M.A. de Souza Silva, B. Topic, J.P. Huston, C. Mattern, Intranasal dopamine application increases dopaminergic activity in the neostriatum and nucleus accumbens and enhances motor activity in the open field, Synapse 62 (3) (2008) 176–184.

[12] T.E. Buddenberg, B. Topic, E.D. Mahlberg, M.A. de Souza Silva, J.P. Huston, C. Mattern, Behavioral actions of intranasal application of dopamine effects on forced swimming elevated plus-maze and open field parameters, Neuropsychobiology 57 (1–2) (2008) 70–79.

[13] M.E. Pum, S. Schäble, H.E. Harooni, B. Topic, M.A. de Souza Silva, J.S. Li, J.P. Huston, C. Mattern, Effects of intranasally applied dopamine on behavioral asymmetries in rats with unilateral 6-hydroxydopamine lesions of the nigro-striatal tract, Neuroscience 162 (1) (2009) 174–183.

[14] L.A. Ruocco, M.A. de Souza Silva, B. Topic, C. Mattern, J.P. Huston, A.G. Sadile, Intranasal application of dopamine reduces activity and improves attention in Naples high excitability rats that feature the mesocortical variant of ADHD, Eur. Neuropsychopharmacol. 19 (10) (2009) 693–701.

[15] O.Y. Chao, C. Mattern, M.A. de Souza Silva, J. Wessler, L.A. Ruocco, S. Nikolaus, J.P. Huston, M.E. Pum, Intranasally applied L-DOPA alleviates parkinsonian symptoms in rats with unilateral nigro-striatal 6-OHDA lesions, Brain Res. Bull. 87 (2012) 340–345.

[16] L.A. Ruocco, C. Treno, U.A. Gironi Carnevale, C.ArraC. Mattern, J.P. Huston, M.A. de Souza Silva, S. Nikolaus, A. Scorziello, M. Nieddu, G. Boatto, P. Illiano, C. Pagano, A. Tino, A.G. Sadile, Prepuberal intranasal dopamine treatment in an animal model of ADHD ameliorates deficient spatial attention working memory amino acid transmitters and synaptic markers in prefrontal cortex ventral and dorsal striatum, Amino Acids 46 (9) (2014) 2105–2122.

[17] S.V. Trossbach, M.A. de Souza Silva, J.P. Huston, C. Korth, C. Mattern, Intranasal dopamine treatment reinstates object-place memory in aged rats, Neurobiol. Learn. Mem. 114 (2014) 231–235.

[18] M.A. Gruden, T.V. Davidova, K. Yanamandra, V.G. Kucheryanu, L.A. Morozova-Roche, V.V. Sherstnev, R.D.E. Sewell, Nasal inoculation with α-synuclein aggregates evokes rigidity, locomotor deficits and immunity to such misfolded species as well as dopamine, Behav. Brain Res. 243 (2013) 205–212.

[19] M.A. Gruden, T.V. Davydova, V.B. Narkevich, V.G. Fomina, C. Wang, V.S. Kudrin, L.A. Morozova-Roche, R.D.E. Sewelle, Intranasal administration of alpha-synuclein aggregates: a Parkinson's disease model with behavioral and neurochemical correlates, Behav. Brain Res. 263 (2014) 158–168.

[20] M.A. Gruden, T.V. Davydova, V.B. Narkevich, V.G. Fomina, C. Wang, V.S. Kudrin, L.A. Morozova-Roche, R.D.E. Sewelle, Noradrenergic and serotonergic neurochemistry arising from intranasal inoculation with α-synuclein aggregates which incite parkinsonian-like symptoms, Behav. Brain Res. 279 (2015) 191–201.

[21] M. Masuda-Suzukake, T. Nonaka, M. Hosokawa, T. Oikawa, T. Arai, H. Akiyama, D.M. Mann, M. Hasegawa, Prion-like spreading of pathological α-synuclein in brain, Brain 136 (Pt 4) (2013) 1128–1138.

[22] R.L. Doty, The olfactory vector hypothesis of neurodegenerative disease: is it viable?, Ann Neurol. 63 (2008) 7–15.

[23] M. Dahlin, U. Bergman, B. Jansson, E. Björk, E. Brittebo, Transfer of dopamine in the olfactory pathway following nasal administration in mice, Pharm. Res. 17 (2000) 737–742.

[24] H. Uchino, Y. Kanai, D.K. Kim, M.F. Wempe, A. Chairoungdua, E. Morimoto, M.W. Anders, H. Endou, Transport of amino acid-related compounds mediated by L-type amino acid transporter 1 (LAT1): insights into the mechanisms of substrate recognition, Mol. Pharmacol. 61 (4) (2002) 729–737.

[25] N. Chemuturi, M.D. Donovan, The Role of Uptake Transporters in Nose to Brain Dopamine Transport: The Characterization of The Role of Dopamine Transporter and Organic Cation Transporter in Dopamine Transport Across the Nasal Mucosa, VDM Verlag, Germany, 2009.

[26] N.V. Chemuturi, M.D. Donovan, Metabolism of dopamine by the nasal mucosa, J. Pharm. Sci. 95 (2006) 2507–2515.

[27] K. Taniguchi, T. Arai, K. Ogawa, Enzyme histochemistry of the olfactory and vomeronasal sensory epithelia in the golden hamster, J. Vet. Med. Sci. 54 (1992) 1007–1016.

[28] S.K.S. Kushwaha, R.K. Keshari, A.K. Rai, Advances in nasal trans-mucosal drug delivery, J. Appl. Pharm. Sci. 1 (2011) 21–28.

[29] L. Illum, Nasal drug delivery – recent developments and future prospects, J. Controlled Release 161 (2012) 254–263.

[30] K. Ikeda, K. Murata, M. Kobayashi, K. Noda, Enhancement of bioavailability of dopamine via nasal route in beagle dogs, Chem. Pharm. Bull. 40 (1992) 2155–2158.

[31] T. Yang, A. Hussain, J. Paulson, T.J. Abbruscato, F. Ahsan, Cyclodextrins in nasal delivery of low-molecular-weight heparins: in vivo and in vitro studies, Pharm. Res. 21 (7) (2004) 1127–1136.

[32] A. Mistry, S. Stolnik, L. Illum, Nanoparticles for direct nose-to-brain delivery of drugs, Int. J. Pharm. 379 (2009) 146–157.

[33] J. das Neves, M.F. Bahia, M.M. Amiji, B. Sarmento, Mucoadhesive nanomedicines: characterization and modulation of mucoadhesion at the nanoscale, Expert Opin. Drug Delivery 8 (2011) 1085–1104.

[34] E. De Giglio, A. Trapani, D. Cafagna, L. Sabbatini, S. Cometa, Dopamine-loaded chitosan nanoparticles: formulation and analytical characterization, Anal. Bioanal. Chem. 400 (2011) 1997–2002.

[35] M. Werle, H. Takeuchi, A. Bernkop-Schnürch, Modified chitosans for oral drug delivery, J. Pharm. Sci. 98 (2009) 1643–1656.

[36] A. Trapani, C. Palazzo, M. Contino, M.G. Perrone, N. Cioffi, N. Ditaranto, N.A. Colabufo, M. Conese, G. Trapani, G. Puglisi, Mucoadhesive properties and interaction with P-glycoprotein (P-gp) of thiolated-chitosans and -glycol chitosans and corresponding parent polymers: a comparative study, Biomacromolecules 15 (3) (2014) 882–893.

[37] M.G. Morgese, T. Cassano, S. Gaetani, T. Macheda, L. Laconca, P. Dipasquale, L. Ferraro, T. Antonelli, V. Cuomo, A. Giuffrida, Neurochemical changes in the striatum of dyskinetic rats after administration of the cannabinoid agonist WIN55,212-2, Neurochem. Int. 54 (1) (2009) 56–64.

[38] C.D. Marsden, J.D. Parkes, "On–off" effects in patients with Parkinson's disease on chronic levodopa therapy, Lancet 1 (1976) 292–296.

[39] R.J. Carey, Chronic L-dopa treatment in the unilateral 6-OHDA rat: evidence for behavioral sensitization and biochemical tolerance, Brain Res. 568 (1991) 205–214.

[40] A. Dolphin, P. Jenner, C.D. Marsden, Noradrenaline synthesis from L-DOPA in rodents and its relationship to motor activity, Pharmacol. Biochem. Behav. 5 (4) (1976) 431–439.

[41] A. Trapani, M. Garcia-Fuentes, M.J. Alonso, Novel drug nanocarriers combining hydrophilic cyclodextrins and chitosan, Nanotechnology 19 (2008) 185101/1–185101/10.

[42] A.A. Mahmoud, G.S. El-Feky, R. Kamel, G.E. Awad, Chitosan/sulfobutylether-β-cyclodextrin nanoparticles as a potential approach for ocular drug delivery, Int. J. Pharm. 413 (1–2) (2011) 229–236.

[43] Z. Fülöp, P. Saokham, T. Loftsson, Sulfobutylether-β-cyclodextrin/chitosan nano- and microparticles and their physicochemical characteristics, Int. J. Pharm. 472 (1–2) (2014) 282–287.

[44] J. Park, T.H. Han, K.Y. Lee, S.S. Han, J.J. Hwang, D.H. Moon, S.Y. Kim, Y.W. Cho, *N*-acetyl histidine-conjugated glycol chitosan self assembled nanoparticles for intracytoplasmic delivery of drugs: endocytosis, exocytosis and drug release, J. Controlled Release 115 (2006) 37–45.

[45] A. Aresta, C.D. Calvano, A. Trapani, C.G. Zambonin, E. De Giglio, α-Tocopherol/chitosan-based nanoparticles: Characterization and preliminary investigations for emulsion systems application, J. Nanopart. Res. 16 (2014) 2230.

[46] E. Herlinger, R.F. Jameson, W. Linert, Spontaneous autoxidation of Dopamine, J. Chem. Soc. Perkin Trans. 2 (1995) 259–263.

[47] A. Trapani, S. Di Gioia, N. Ditaranto, N. Cioffi, F.M. Goycoolea, A. Carbone, M. Garcia-Fuentes, M. Conese, M.J. Alonso, Systemic heparin delivery by the pulmonary route using chitosan and glycol chitosan nanoparticles, Int. J. Pharm. 447 (2013) 115–123.

[48] T. Musumeci, R. Pellitteri, M. Spatuzza, G. Puglisi, Nose-to-brain delivery: evaluation of polymeric nanoparticles on olfactory ensheathing cells uptake, J. Pharm. Sci. 103 (2) (2014) 628–635.

[49] T. Cassano, S. Gaetani, M.G. Morgese, T. Macheda, L. Laconca, P. Dipasquale, J. Taltavull, T.S. Shippenberg, V. Cuomo, G. Gobbi, Monoaminergic changes in locus coeruleus and dorsal raphe nucleus following noradrenaline depletion, Neurochem. Res. 34 (2009) 1417–1426.

[50] H. Ikeda, M. Nakamura, N. Ise, F. Toda, A. Ueno, NMR Studies of conformations of *N*-dansyl-l-leucine-appended and *N*-dansyl-d-leucine-appended β-cyclodextrin as fluorescent indicators for molecular recognition, J. Org. Chem. 62 (5) (1997) 1411–1418.
[51] W.G. Meissner, M. Frasier, T. Gasser, C.G. Goetz, A. Lozano, P. Piccini, J.A. Obeso, O. Rascol, A. Schapira, V. Voon, D.M. Weiner, F. Tison, E. Bezard, Priorities in Parkinson's disease research, Nat. Rev. Drug Discov. 10 (5) (2011) 377–393.
[52] S. Md, S. Haque, M. Fazil, M. Kumar, S. Baboota, J.K. Sahni, J. Ali, Optimised nanoformulation of bromocriptine for direct nose-to-brain delivery: biodistribution, pharmacokinetic and dopamine estimation by ultra-HPLC/mass spectrometry method, Expert Opin. Drug Delivery 11 (6) (2014) 827–842.
[53] J. Panyam, S.K. Sahoo, S. Prabha, T. Bargar, V. Labhasetwar, Fluorescence and electron microscopy probes for cellular and tissue uptake of poly (D,L-lactide-co-glycolide) nanoparticles, Int. J. Pharm. 262 (2003) 1–11.
[54] A. Trapani, V. Laquintana, A. Lopedota, M. Franco, A. Latrofa, G. Talani, E. Sanna, G. Trapani, G. Liso, Evaluation of new propofol aqueous solutions for intravenous anesthesia, Int. J. Pharm. 278 (2004) 91–98.
[55] J. Szejtli, Introduction and general overview of cyclodextrin chemistry, Chem. Rev. 98 (5) (1998) 1743–1754.
[56] H.J. Schneider, F.F. Hacket, V. Rüdiger, H. Ikeda, NMR studies of cyclodextrins and cyclodextrin complexes, Chem. Rev. 98 (5) (1998) 1755–1786.
[57] B.A. McLaughlin, D. Nelson, M. Erecińska, M.F. Chesselet, Toxicity of dopamine to striatal neurons in vitro and potentiation of cell death by a mitochondrial inhibitor, J. Neurochem. 70 (6) (1998) 2406–2415.
[58] D.G. Graham, Catecholamine toxicity: a proposal for the molecular pathogenesis of manganese neurotoxicity and Parkinson's disease, Neurotoxicology 5 (1) (1984) 83–95.
[59] D.G. Graham, S.M. Tiffany, W.R. Bell Jr., W.F. Gutknecht, Autoxidation versus covalent binding of quinones as the mechanism of toxicity of dopamine, 6-hydroxydopamine, and related compounds toward C1300 neuroblastoma cells in vitro, Mol. Pharmacol. 14 (4) (1978) 44–53.
[60] L. Chen, Y. Ding, B. Cagniard, A.D. Van Laar, A. Mortimer, W. Chi, T.G. Hastings, U.J. Kang, X. Zhuang, Unregulated cytosolic dopamine causes neurodegeneration associated with oxidative stress in mice, J. Neurosci. 28 (2008) 425–433.
[61] C.L. Graff, G.M. Pollack, Nasal drug administration: potential for targeted central nervous system delivery, J. Pharm. Sci. 94 (2005) 1187–1195.
[62] S.V. Dhuria, L.R. Hanson, W.H. Frey, Intranasal delivery to the central nervous system: mechanisms and experimental considerations, J. Pharm. Sci. 99 (2010) 1654–1673.